



## On the local anthropogenic source diversities and transboundary transport for urban agglomeration ozone mitigation

Yingying Yan<sup>a</sup>, Huang Zheng<sup>a,b</sup>, Shaofei Kong<sup>a,\*</sup>, Jintai Lin<sup>c,\*\*</sup>, Liquan Yao<sup>a,b</sup>, Fangqi Wu<sup>a</sup>, Yi Cheng<sup>a</sup>, Zhenzhen Niu<sup>a</sup>, Shurui Zheng<sup>a</sup>, Xin Zeng<sup>b</sup>, Qin Yan<sup>a,b</sup>, Jian Wu<sup>a,b</sup>, Mingming Zheng<sup>b,d</sup>, Mengyao Liu<sup>c</sup>, Ruijing Ni<sup>c</sup>, Lulu Chen<sup>c</sup>, Nan Chen<sup>d</sup>, Ke Xu<sup>d</sup>, Dantong Liu<sup>e</sup>, Delong Zhao<sup>f</sup>, Tianliang Zhao<sup>g</sup>, Shihua Qi<sup>b</sup>

<sup>a</sup> Department of Atmospheric Science, School of Environmental Sciences, China University of Geosciences, Wuhan, 430074, China

<sup>b</sup> Department of Environmental Science and Technology, School of Environmental Sciences, China University of Geosciences, Wuhan, 430074, China

<sup>c</sup> Laboratory for Climate and Ocean-Atmosphere Studies, Department of Atmospheric and Oceanic Sciences, School of Physics, Peking University, Beijing, 100871, China

<sup>d</sup> Hubei Environmental Monitoring Centre, Wuhan, 430072, China

<sup>e</sup> Department of Atmospheric Sciences, School of Earth Sciences, Zhejiang University, Hangzhou, Zhejiang, China

<sup>f</sup> Beijing Weather Modification Office, Beijing, 100089, China

<sup>g</sup> School of Atmospheric Physics, Nanjing University of Information Science and Technology, Nanjing, 210044, China

### HIGHLIGHTS

- Distinct city-level characteristics in ozone and precursors are found.
- Substantial variabilities are found in photochemical formation of ozone across the cities and days.
- Removing a city's local anthropogenic emissions alone can effectively mitigate ozone pollution.

### ARTICLE INFO

#### Keywords:

Ozone mitigation  
Urban agglomeration pollution  
Local source diversities  
Transboundary transport  
Ozone modeling

### ABSTRACT

Mitigation of ozone in urban agglomerations of developing countries remains challenging, due partly to inadequate knowledge of the relative importance of local sources versus transboundary transport, aggravated by lack of synchronous measurements of ozone and precursors. Here we investigate the spatial-temporal characteristics of ozone and its precursors measured synchronously at five cities of Wuhan City Cluster (WCC) in Central China during the high-ozone months of May–June 2018, facilitated by multiple models of different complexities. We find substantial cross-city diversities in the measured maximum daily averaged 8-h (MDA8) ozone, nitrogen oxides ( $\text{NO}_x = \text{NO} + \text{NO}_2$ ), volatile organic compounds (VOCs), VOCs/ $\text{NO}_x$  ratios, and ozone formation potentials of VOCs, which are tied to distinctive local emission sources. GEOS-Chem simulations suggest that local anthropogenic emissions contribute 26.8–29.5% of ozone in each city averaged over May–June 2018, with higher values during ozone episodes (up to 32.0%). Transboundary transport from non-WCC Asian regions (18.5–19.2%) contributes much more than cross-city transport within WCC (2.5–3.1%) to ozone concentrations in the five cities. The contributions of background ozone from non-Asian anthropogenic emissions and global natural sources reach 48.9–51.6%. Thus local mitigation actions alone can substantially reduce city-level ozone; whereas the majority of ozone must be mitigated by country-wide or worldwide collaborations. Collaborations within an urban agglomeration alone may not effectively mitigate ozone.

\* Corresponding author.

\*\* Corresponding author.

E-mail addresses: [kongshaofei@cug.edu.cn](mailto:kongshaofei@cug.edu.cn) (S. Kong), [linjt@pku.edu.cn](mailto:linjt@pku.edu.cn) (J. Lin).

## 1. Introduction

Surface ozone ( $O_3$ ) is a harmful pollutant affecting human health (Lelieveld et al., 2015), vegetation growth (Monks et al., 2015) and crop yields (Tai et al., 2004). It is mainly produced by photochemical processes involving  $NO_x$ , non-methane volatile organic compounds (NMVOCs) and carbon monoxide (CO), and is removed from the atmosphere by chemical depletion and dry deposition (Monks et al., 2015). In addition, stratospheric ozone may also affect the tropospheric ozone budget (Zhang et al., 2015; Verstraeten et al., 2015; Zhang Tianet al., 2018). Despite efforts to control ozone, summertime ozone concentrations in the Northern Hemisphere continue to exceed ambient air quality standards (Li et al., 2019a; Sun et al., 2019; Yan et al., 2018a, 2018b). The exceedances can pose severer threat to human society in urban agglomerations than that in other regions. European Environment Agency (EEA, 2017) has reported that 90% of the urban population is exposed to ozone exceeding the WHO guideline (EEA, 2017).

The abatement of surface ozone through precursor ( $NO_x = NO + NO_2$ , and VOCs) controls faces difficulties for urban agglomerations (Li et al., 2019b). From 1997 to 2010, a reduction ratio of 3:1 in anthropogenic VOC-to- $NO_x$  was recommended to be used for urban areas of the Pearl River Delta (PRD) in the Guangdong–Hong Kong Joint Emission Reduction Plan (Ou et al., 2016). Such a VOC reduction plan proved not successful due to VOC sources in the PRD being too scattered and diverse to be controlled effectively. Even over Europe and the US, although peak ozone levels in rural areas have been declining due to precursor emission controls applied to the VOCs and  $NO_x$  emissions (Yan et al., 2018a, 2018b; Derwent et al., 2010), ozone concentration in urban regions is towards an increase (Yan et al., 2018b; Wilson et al., 2012; Colette et al., 2011).

Following the first generation of ozone reduction strategies (EEA, 2007; EEA, 2009; EEA, 2011; Royal Society, 2008; Fowler et al., 2013) focused on local precursor emission controls, long-range transboundary transport of ozone and its precursors have been highlighted to make significant contributions to the exceedance of air quality standards (Ni et al., 2018; HTAP, 2010; Lin et al., 2008). As regional collaborative mitigation actions are typically more difficult to be agreed upon or conducted than local unilateral actions, it becomes crucial for urban agglomerations to understand to what extent local mitigation actions may be effective.

Concurrent measurements of ozone and precursors have been used to identify ozone sources, elucidate ozone-forming regimes (So and Wang, 2004; Cheung and Wang, 2001; Xue et al., 2014) and apportion sources of VOCs (Guo et al., 2004, 2006; Geng et al., 2007, 2010). A large number of studies have been done on field measurements of ozone and impacts of precursor emissions on ozone pollution in megacities over urban agglomeration regions (Monks et al., 2015; So and Wang, 2003, 2004; Wang et al., 2010; Han et al., 2011). However, synchronized station measurements of ozone and its precursors are relatively rare on an urban agglomeration scale in developing countries (Monks et al., 2015). This limits the understanding of ozone-precursors relationship specific for each city, which is important for ozone mitigation.

To analyze the effectiveness of local mitigation at each city for regional ozone pollution on an urban agglomeration scale, we shall first resolve the ozone sources of local formation versus transboundary transport. Thus sensitivity simulations by a chemical transport model are essential to be conducted for ozone source attribution (Ni et al., 2018; Yan et al., 2019a). Moreover, elucidating ozone-forming regimes for each city and apportioning sources of VOCs at individual city are practically significant for local mitigation actions. To identify ozone-formation regimes, previous studies often adopt a box model associated with observed VOCs/ $NO_x$  ratios (So and Wang, 2004; Cheung and Wang, 2001; Xue et al., 2014). A receptor model is usually reported to be used to conduct VOCs source apportionment (Guo et al., 2004, 2006; Geng et al., 2007, 2010).

Here we investigate the relative contributions of local emissions and

transboundary transport of different scales to city-level ozone in the pollution-loaded five cities of Wuhan City Cluster (WCC) in Central China (the middle reach of the Yangtze River). WCC with sub basin topography is surrounded by major pollution areas in China, the Northern China Plain (NCP) to the north, the Yangtze River Delta (YRD) to the east, the PRD to the south, and the Sichuan Basin (SCB) to the west (Fig. S1). Thus WCC is a regional pollutant transport hub with transportation-pollution characteristics. This region is reported to be affected by two transport pathways from the NCP region (Zheng et al., 2019) and from the vast flatland in central eastern China (Yu et al., 2020). In combination with high anthropogenic emissions and secondary pollution formation, WCC often suffers severe ozone pollution episodes. The study is based on synchronous hourly measurements of ozone and its precursors in the five cities during May–June in 2018, together with a box model for the ozone chemistry, a receptor model for VOC source characterization, and a chemical transport model for ozone source attribution.

## 2. Data and methods

In a few steps, we differentiate the individual contributions of local anthropogenic sources and transboundary transport to ozone at each of the five cities in WCC in May–June 2018. We first quantify the spatial and temporal variations of ozone and its precursors. We also elucidate the ozone photochemical production regimes at individual cities based on measured VOCs/ $NO_x$  ratios and DSMACC (Dynamically Simple Model for Atmospheric Chemical Complexity) chemistry box model simulations. We then conduct VOCs source apportionment through the Positive Matrix Factorization (PMF) model. At last, we conduct sensitivity simulations of GEOS-Chem model to quantify the individual effects of local anthropogenic emissions and transboundary transport on ozone at each city.

### 2.1. Data

Hourly measurement data of ozone and its precursors ( $NO$ ,  $NO_2$ , and VOCs) at five cities are provided by the Hubei Province Environmental Quality Monitoring Data Management Platform. There is one measurement site for each city (Wuhan: WH, 30.53°N, 114.37°E; Xiaogan: XG, 30.90°N, 113.94°E; Huangshi: HS, 30.20°N, 115.08°E; Huanggang: HG, 30.44°N, 114.89°E; Ezhou: EZ, 30.36°N, 114.90°E; data is available at <http://59.172.208.250:8082/Login/index>) (Fig. S1). All sites are located at residential/commercial areas.

The hourly VOCs observations include 102 species, which are measured using online GC-MS/FID system (TH-300B, Wuhan Tianhong Instrument Co. Ltd, China). Briefly, ambient air is collected at a flow rate of 60 ml  $min^{-1}$  with the moisture and carbon dioxide removed at cold traps at  $-80^\circ C$  and  $-150^\circ C$ , respectively. The pre-cleaned air is then concentrated to 300 ml using an electronic refrigeration system. The concentrated air is subsequently desorbed quickly by heating to  $100^\circ C$  and then introduced into a chromatographic column. Double chromatographic systems are used to separate VOCs, with low molecular weight hydrocarbons ( $C_2$ – $C_5$ ) extracted by a nonpolar capillary column (PLOT- $Al_2O_3$ , length: 15 m, diameter: 0.32 mm, thickness of membrane: 3  $\mu m$ ) and high molecular weight VOCs ( $C_6$ – $C_{12}$ ) by a semi-polar column (DB-624, length: 60 m, diameter: 0.25 mm, thickness of membrane: 1.4  $\mu m$ ). Individual  $C_2$ – $C_5$  species are then determined by a FID detector, and  $C_6$ – $C_{12}$  species by a mass spectrum detector. For quality control, the daily calibration is usually operated at 00:00 local time using a known mixing ratio standard gas (2 ppbv) containing 55 VOC species to be used in the PMF model. More details about the instrument and data quality control can be found elsewhere (Lyu et al., 2016).

### 2.2. DSMACC box model simulation

The DSMACC box model is used to simulate the formation of ozone

under different concentrations of VOCs and NO<sub>x</sub>, in order to illustrate the nonlinear characteristics of the O<sub>3</sub>-VOCs-NO<sub>x</sub> reaction system. The simulation of DSMACC with the chemical mechanism of GEOS-Chem is set to clear sky at noon (12:00–13:00) in June. During this period of noon, both the ozone generation efficiency and the ozone concentration are the highest in a day. Additionally, DSMACC box model with GEOS-Chem chemical mechanism has much larger bias in the modeled nighttime ozone than the daytime ozone (Yan et al., 2019b, 2019c). Necessary meteorological inputs are set based on the mean values of measurements in individual city, including surface air pressure, air temperature, water vapor content, and solar radiation. The initial concentrations for ozone and CO are also set based on the observed mean values. VOCs and NO<sub>x</sub> concentrations at each city are set based on the GEOS-Chem simulations.

### 2.3. Receptor model

The PMF model is adopted for the source apportionment of 55 VOC species; see Supplementary Sect. S1 for details. The receptor matrix is based on the hourly VOCs observation data at each site. The criteria to select VOC species for the PMF model follows Zheng et al. (2018)<sup>34</sup>: (1) detection rate > 60%; (2) signal to noise ratio (S/N) > 0.2; (3) species with good correlations; (4) VOCs species can be used as an indicator of a certain source. Details of the input species for the PMF model are shown in the captions of Figs. S2–S6. Choosing the optimal number of factors (i.e., VOC species) in PMF is always challenging. Too many factors would result in meaningless sources, whereas too few factors would lead to mixed sources for a factor. Therefore, the number of factors is tested from 3 to 8 to find the optimal number for each city. The bootstrap and displacement techniques are used to test the robustness of the solutions. More details about the PMF operation can be found elsewhere (Zheng et al., 2018a).

### 2.4. GEOS-chem simulation

Ozone and its precursors concentrations over Central China are simulated using a nested GEOS-Chem model v11-02 (<http://acmg.seas.harvard.edu/geos/>). The nested model, covering China (70°E–140°E, 15°S–55°N), is run from April 15th to June 30th, 2018. The simulation in April is used for model spin-up, and the results in May–June are used for analysis. The model is run with a horizontal resolution of 0.25° latitude × 0.3125° longitude and 47 vertical layers, with 10 layers (each ~130 m in thickness) below 850 hPa. Although the spatial resolution of this model is relatively coarse to conduct simulations of WCC, such horizontal resolution is the finest grid for GEOS-Chem nested model over China. In order to represent these five cities, simulation results are averaged over the grids covered by the entire urban area of individual city. The model is driven by the GEOS-FP assimilated meteorological data. GEOS-Chem includes detailed tropospheric Ozone-NO<sub>x</sub>-VOCs-HO<sub>x</sub> chemistry (Mao et al., 2013), online aerosol calculations, the Linoz stratospheric ozone generation mechanism (McLinden et al., 2000), and a non-local scheme for planetary boundary layer mixing (Lin and McElroy, 2010). Monthly anthropogenic emissions of carbon monoxide (CO), NO<sub>x</sub> and VOCs over China are taken from the Multi-resolution Emission Inventory (MEIC, <http://meicmodel.org>) for 2016, the latest year in which Chinese emission data are available. Other emission treatments are presented in Supplementary Sect. S2. The simulation results are evaluated with measurements of ozone and its precursors at the five sites. Sensitivity simulations are further conducted to differentiate the effects of transboundary transport and local anthropogenic emissions on city-level ozone concentrations.

## 3. Results

### 3.1. Observed cross-city consistency and differences in ozone and precursors

Fig. 1a shows the maximum daily averaged 8-h (MDA8) ozone at the five sites from May to June 2018. MDA8 ozone concentrations change substantially from one day to another, with the highest values on June 16 (220.7–275.1 μg m<sup>-3</sup> across the cities) and the lowest on May 20 (32.2–73.6 μg m<sup>-3</sup>). Ozone pollution is severe on many days of this time period. On June alone, the number of days in which MDA8 ozone concentrations exceed China's Grade II standard (160 μg m<sup>-3</sup>) are 14 (47%), 8 (27%), 12 (40%), 16 (53%) and 12 (40%) days at WH, HS, EZ, XG and HG, respectively. The ozone episodes are most evident during June 1–21.

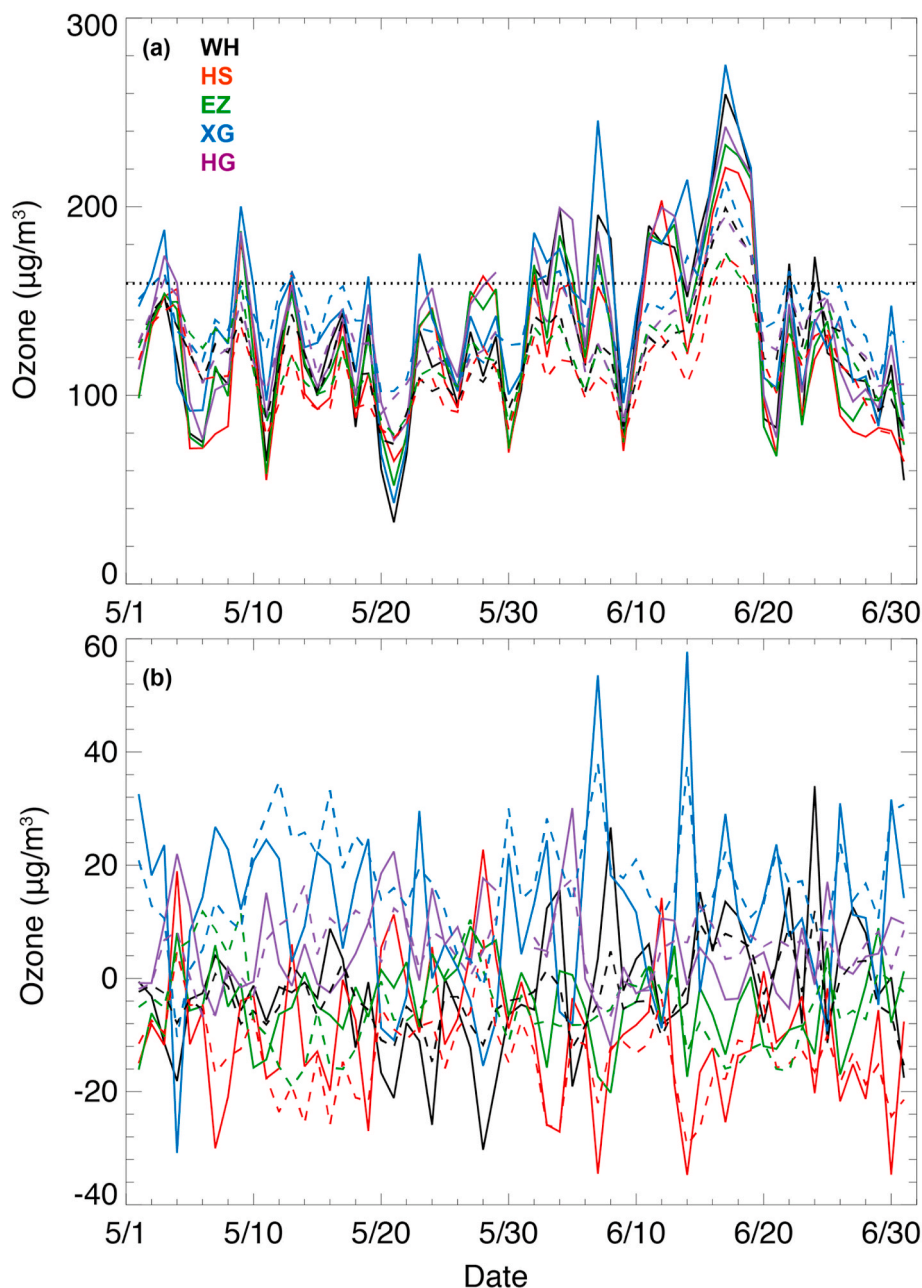
Although there is large consistency in MDA8 ozone temporal variations at these five cities (R = 0.87–0.95 between any two cities, P-value < 0.01), there is substantial cross-city difference on each day. By removing the 5-city average on each day, Fig. 1b better shows the cross-city ozone differences. In particular, the correlation coefficients of MDA8 anomalies between any two cities (−0.23–0.19) become statistically insignificant. The range of cross-city difference is about 0.1–92.4 μg m<sup>-3</sup>, with an average of 16.6 μg m<sup>-3</sup>. The largest cross-city difference occurs between HS and XG on June 6 and June 13, with values reaching 88.6 and 92.4 μg m<sup>-3</sup>. The consistency and diversities of ozone concentrations at the five cities suggest that ozone pollution over WCC is of regional characteristic but with substantial influences from local sources within each city.

Fig. 2 shows the measured time series of daytime (10:00–15:00 local time) mean VOCs, NO<sub>x</sub>, NO<sub>2</sub> and NO concentrations between May 1 and June 30 at the five sites. In contrast to the relatively spatially consistent daily variation of ozone, the day-to-day variations of NO<sub>x</sub>, NO<sub>2</sub>, NO and VOCs differ from one city to another. On some days, the VOCs concentrations differ by a factor of 6 across the five sites, NO<sub>2</sub> by one order of magnitude, and NO by two orders of magnitude. NO concentrations in several pollution episodes (17 ± 11 μg m<sup>-3</sup> across the five sites) are much higher than the temporally averaged value (3.3 ± 2.9 μg m<sup>-3</sup>).

Table 1 further shows the observed concentrations of ozone and precursors averaged over May–June at the five sites. The temporal average ozone concentrations are similar at these five sites (122.7–144.2 μg m<sup>-3</sup>). In contrast, the temporal average concentrations of NO<sub>x</sub> range drastically from 15.5 to 37.0 μg m<sup>-3</sup>. The cross-city range of VOCs concentrations is also large, i.e., from 60.3 to 118.5 μg m<sup>-3</sup>. The NO<sub>x</sub> and VOCs results further suggest cross-city diversity in local ozone formation.

The black dots in Fig. 3 represent the hourly observed VOCs and NO<sub>x</sub> concentrations during the strong ozone photochemical buildup hours (10:00–15:00) at individual cities and hours for investigation of the ozone formation regime. The observed daytime (10:00–15:00 local time) VOCs/NO<sub>x</sub> ratios range from 0.8 to 13.7 across the cities and hours. Averaged over May–June, the VOCs/NO<sub>x</sub> ratios range from 2.5 to 6.1 across the five cities (Table 1). The filled contours in Fig. 3 further show the ozone isopleth diagrams for the five cities based on simulations of the photochemical box model DSMACC (Gressent et al., 2016). The DSMACC simulated VOCs/NO<sub>x</sub> ratios on the ridge line that connects maximum ozone formation values are between 7.6 and 9.6 (Fig. 3), larger than the observed temporal average ratios (2.5–6.1) at these cities. Therefore, on average, the ozone formation is VOC-limited at these cities. Nonetheless, the VOCs/NO<sub>x</sub> ratios vary substantially across the days and cities, and may even become below the DSMACC simulated VOCs/NO<sub>x</sub> ratio ridge line, i.e., in the NO<sub>x</sub>-limited regime (Fig. 3).

Meteorological parameters (temperature, humidity and wind, etc.) can influence O<sub>3</sub> concentrations via mechanisms related to transport, chemical production and loss, and deposition (Ni et al., 2018; Yan et al., 2019a). From the correlation between the observed ozone concentrations to the measured meteorological factors (air temperature and



**Fig. 1.** (a) Time series of observed (solid lines) and modeled (dashed lines) MDA8 ozone concentrations in the five cities. The black dotted line shows China's Secondary Standard ( $160 \mu\text{g m}^{-3}$ ). (b) MDA8 ozone anomalies after removing the 5-city average.

relative humidity; Fig. S9), it could be found that ozone concentrations over these five cities are highly dependent on the meteorological fields, with correlation coefficients of 0.75–0.78 ( $P$ -value  $< 0.01$ ) for temperature and of  $-0.80$ – $0.86$  for humidity ( $P$ -value  $< 0.01$ ). However, from the statistical comparisons in meteorological factors of the five cities shown in Table S2, the differences in meteorological fields in the five cities are relatively small. Thus following we mainly discuss the local anthropogenic source diversities and transboundary transport to understand the differences in ozone in these cities.

### 3.2. Cross-city diversities of VOC sources and their contributions to ozone formation potential

Using the PMF model, we identify seven VOC sources, including fuel evaporation (FE), vehicle emissions (VE), industrial sources (IS, including oil refinery and industry production), solvent usage (SU),

combustion sources (CS), biogenic sources (BIO), and other mixed sources (MIX). Not all sources are found in a city – there are four VOCs sources for HG, five sources for EZ, and six sources for HS, WH and XG. The source profiles and diurnal variations derived from the PMF model at the five sites are shown in Figs. S2–S6. The source identification results are consistent with previous reports of potential sources of individual VOC species (Table S1). To understand the relative contributions of individual VOC sources to the ozone formation potential (OFP), we combine the maximum incremental reactivity-weighted (MIR) concentration calculation and the PMF model (Zheng et al., 2018a). Hereafter, we will discuss the diversities of VOC sources and their contributions to OFP at the five cities.

Fig. 4 shows that five VOCs sources are identified at WH. Specifically, FE accounts for the highest fraction (40.3%) to the total VOCs mixing ratio, followed by VE (33.0%), MIX (11.2%), BIO (8.66%), and IS (6.84%). The contributions to the ozone formation potential of FE, VE,

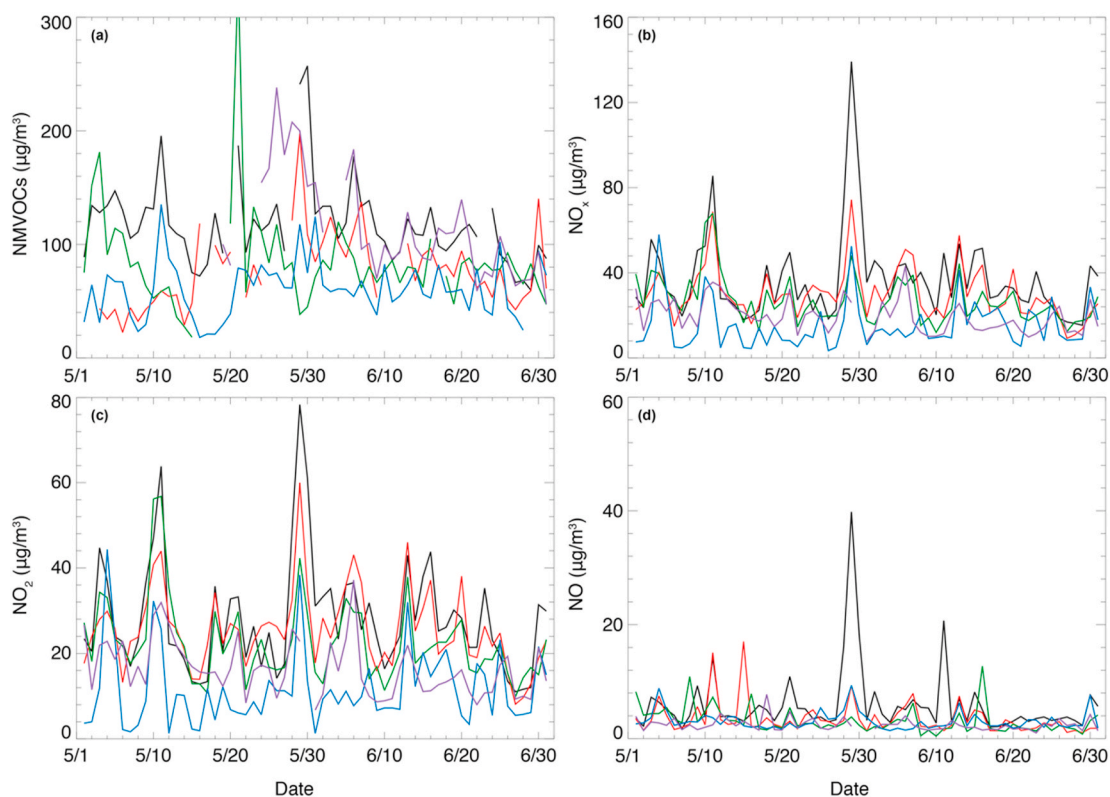


Fig. 2. Measured time series of daytime (10:00–15:00 local time) mean VOCs (a),  $\text{NO}_x$  (b),  $\text{NO}_2$  (c) and NO (d) concentrations in May and June in the five cities.

MIX, BIO, and IS are 36.8%, 21.7%, 18.7%, 12.4% and 10.3%, respectively. FE here includes fugitive emissions from liquid petroleum gas and gasoline evaporation. The liquid petroleum gas source is identified according to the high abundances of propane and butanes in source composition (Liu et al., 2008; Bon et al., 2011), and gasoline evaporation is identified according to the high loadings on *i*-pentanes (Gentner et al., 2009; Zhang et al., 2013). VE are associated with abundant acetylene, a tracer of combustion in vehicle engines (McCarthy et al., 2013). High percentages of ethane, propane, ethene, propene, toluene, ethylbenzene, and xylenes are also found from VE (Liu et al., 2008; Zhang et al., 2018). This VE source is identified with a clear diurnal cycle: two peaks at about 08:00 and 20:00 local time, associated with traffic rush hours, and a minimum at about 15:00 (Fig. S2).

The MIX source at WH is associated with high percentages of  $\text{C}_6$ – $\text{C}_8$  alkanes, such as methycyclopentane, methycyclohexane and cyclohexane from the petrochemical industry, as well as hexane, heptane, 2-methylheptane, 3-methylheptane from solvent usage. Toluene, ethylene and xylenes are also found as the abundant fractions in MIX. BIO is identified according to isoprene, a tracer of biogenic emissions (Derstroff et al., 2016; Kaltsonoudis et al., 2016). The diurnal variation of this source shows higher levels during daytime than nighttime, with a rapid increase after sunrise and a peak value in the afternoon (about 15:00 local time). IS is identified by heavy loadings only of ethene and propene, which indicate the petrochemical industry production (Liu et al., 2008; Jobson, 2004; Song et al., 2018) (Fig. S2).

XG has one additional source identified besides those five for WH. The sixth source, SU, is identified by high loadings of toluene, ethylbenzene, *m/p*-xylenes and *o*-xylenes (Wang, 2014; Yuan et al., 2010). IS accounts for the highest fraction (35.8%) to the total VOCs mixing ratio, with high loadings of ethane, propane, cyclohexane, 2,2,4-methylpentane, toluene, ethylene and xylenes related to industry production (Liu et al., 2008; Song et al., 2018). The second largest contributor (26.1%) to the total VOCs mixing ratio is VE. Although SU contributes much less to the VOCs mixing ratio (9.3%) than IS and VE do, its contribution to

the OFP (23.9%) is much higher than IS (14.2%) and comparable to that of VE (26.6%).

A total of 6 sources are identified at HS, including VE, FE, SU, MIX, BIO and IS. Here, SU accounts for the highest fraction (34.6%) of the OFP but a relatively low percentage (15.4%) of the total VOCs mixing ratio, similar to the case in XG. Different from XG and WH, HS has the highest contribution to the total VOCs mixing ratio from VE (27.7%), although VE contributes less (15.0%) to the OFP.

At HG, only four VOCs sources are identified, including FE, VE, MIX and BIO. FE and VE are the dominant contributors to the total VOCs mixing ratio (39.6% and 28.9%) as well as the OFP (32.3% and 31.0%). EZ has one special source, CS, identified that is associated with high loadings of propane and acetylene from combustion (McCarthy et al., 2013). This CS source accounts for the highest fraction of the total VOCs mixing ratio (29.6%), although its contribution to the OFP (12.3%) is less than VE (27.9%).

### 3.3. Contribution of local anthropogenic sources versus transboundary transport to city-level ozone

To better understand the causes of ozone pollution at each city, we further use the GEOS-Chem model to simulate the individual contributions of local anthropogenic emissions and transboundary atmospheric transport. Our “Control” simulation (with natural and anthropogenic emissions over whole region; Table 3 shows the anthropogenic emissions of ozone precursors (CO,  $\text{NO}_x$  and VOCs) for the five cities in GEOS-Chem during May–June in 2018; Fig. 5 further shows the actual boundaries of these five cities with the GEOS-Chem model grid cells and MEIC emission shown explicitly.) reproduces the observed temporal variation of MDA8 ozone data at the five sites (Fig. 1a), with statistically significant model-observation correlations (0.82–0.92,  $P$ -value < 0.01; Table 1). In contrast to the reported model overestimation at non-urban (rural/regional background) sites over China (Sun et al., 2019; Ni et al., 2018), the model results at these five urban sites in WCC are generally

**Table 1**

Summary of the statistical comparisons between observed and simulated concentrations ( $\mu\text{g m}^{-3}$  for  $\text{O}_3$ , VOCs<sup>a</sup>,  $\text{NO}_x$ ,  $\text{NO}_2$ , and  $\text{NO}$ ) at the five sites. MDA8 values are presented for  $\text{O}_3$ , and daytime mean values for VOCs,  $\text{NO}_x$ ,  $\text{NO}_2$ , and  $\text{NO}$ . MMOD and MOBS represent the mean values for the “Control” simulation and the observation, respectively. MB is the mean model bias defined as  $\text{MMOD} - \text{MOBS}$ . NMB is the normalized mean bias of model results defined as:  $(\text{MMOD} - \text{MOBS})/\text{MOBS}$ . SMOD and SOBS are their standard deviations. TCOR is the temporal correlations between model results and measurements.

Sites	Species	MMOD	MOBS	SMOD	SOBS	TCOR
		(MB, NMB)				
WH	$\text{O}_3$	123.1 (−7.4; −5.7%)	130.5	26.5	42.9	0.80
	VOCs	74.7 (−43.3; −36.8%)	117.7	29.7	36.8	0.62
	$\text{NO}_x$	48.9 (11.9; 32.2%)	37.0	20.2	22.8	0.69
	VOCs/ $\text{NO}_x$	2.3 (−0.9; −28.1%)	3.2	1.0	1.2	0.63
	$\text{NO}_2$	35.7 (7.5; 26.6%)	28.2	17.3	15.5	0.69
	$\text{NO}$	9.9 (4.0; 54.5%)	5.9	11.7	9.4	0.54
XG	$\text{O}_3$	143.3 (−1.0; −0.7%)	144.2	28.5	46.2	0.82
	VOCs	46.7 (−13.6; −22.6%)	60.3	20.4	24.6	0.58
	$\text{NO}_x$	19.4 (3.9; 43.1%)	15.5	13.4	11.5	0.71
	VOCs/ $\text{NO}_x$	2.4 (−1.5; 38.4%)	3.9	1.8	2.6	0.59
	$\text{NO}_2$	15.5 (4.2; 67.1%)	11.3	11.2	9.8	0.72
	$\text{NO}$	2.9 (−0.2; −4.1%)	3.1	1.6	1.6	0.48
HS	$\text{O}_3$	112.3 (−10.4; −8.5%)	122.7	21.3	48.1	0.84
	VOCs	52.8 (−22.8; −30.2%)	75.6	25.4	33.9	0.51
	$\text{NO}_x$	39.5 (9.3; 38.5%)	30.3	15.1	12.4	0.61
	VOCs/ $\text{NO}_x$	1.4 (−1.1; −44.0%)	2.5	0.5	0.8	0.51
	$\text{NO}_2$	34.6 (8.9; 42.7%)	25.6	11.1	10.6	0.62
	$\text{NO}$	3.8 (0.3; 28.2%)	3.5	2.9	3.4	0.29
HG	$\text{O}_3$	131.8 (−7.1; −5.1%)	138.9	23.7	45.2	0.78
	VOCs	78.7 (−39.8; −33.6%)	118.5	33.3	51.8	0.51
	$\text{NO}_x$	25.6 (6.1; 31.3%)	19.5	13.4	12.0	0.63
	VOCs/ $\text{NO}_x$	3.3 (−2.8; −45.3%)	6.1	1.6	2.7	0.53
	$\text{NO}_2$	23.1 (6.7; 40.8%)	16.4	6.5	8.4	0.70
	$\text{NO}$	2.1 (−0.3; −7.90%)	2.4	1.1	1.1	0.37
EZ	$\text{O}_3$	120.8 (−7.2; −5.6%)	128.0	25.9	48.2	0.83
	VOCs	56.6 (−27.9; −32.9%)	84.8	25.1	44.3	0.68
	$\text{NO}_x$	38.7 (11.7; 49.3%)	27.1	16.3	15.7	0.57
	VOCs/ $\text{NO}_x$	1.7 (−1.4; −44.9%)	3.1	0.9	1.3	0.57
	$\text{NO}_2$	33.1 (10.6; 54.5%)	22.6	12.1	13.3	0.67
	$\text{NO}$	4.4 (1.3; 55.1%)	3.2	2.5	4.8	0.31

<sup>a</sup> Observed VOC species are listed in the captions of Figs. S2–S6; modeled VOC species includes benzene, toluene, xylene, isoprene, other alkenes, ethane, propane, other alkanes, formaldehyde, other aldehydes, acetone and methyl ethyl ketone.

underestimated especially during high ozone concentration events (Fig. 1a), with an average underestimate of 1.0–10.4  $\mu\text{g m}^{-3}$  (0.7–8.5%; Table 1). The difference in modeled biases at non-urban and urban sites may be explained by the different artificial dispersion of localized  $\text{NO}_x$  emissions in non-urban and urban regions caused by the grid resolution applied in GEOS-Chem model (Yan et al., 2019c). Moreover, the diversities of ozone concentrations at the five cities are well captured by the model, with the cross-city differences of 0.1–44.7  $\mu\text{g m}^{-3}$  (Fig. 1b). Model evaluation of other regions is not shown due to lack of measurements during May–June in 2018. Ni et al. (2018) have evaluated the GEOS-Chem simulation over China and its neighboring area using a suite of ground measurements during 2007–2008 and showed an overall small bias for ozone near the surface (10% at 10 surface sites with hourly measurements, 15% at 21 surface sites with monthly observations). Global ozone evaluation of the GEOS-Chem model is detailed in Yan

et al. (2016) using 1420 ground sites measurements in 2009. The model can reproduce the observed day-to-day variation of afternoon mean surface  $\text{O}_3$  with an averaged correlation of 0.53 and a mean model bias of 10.8 ppb.

Table 1 and Fig. S7 also evaluate the modeled daytime averaged  $\text{NO}_x$ ,  $\text{NO}_2$ ,  $\text{NO}$  and VOCs concentrations and the VOCs/ $\text{NO}_x$  ratio at these five sites. The “Control” simulation reproduces the variabilities in daytime observation data fairly well, with the highest correlations for  $\text{NO}_2$  ( $R = 0.62$ – $0.72$ ), followed by  $\text{NO}_x$  ( $R = 0.57$ – $0.71$ ), VOCs ( $R = 0.51$ – $0.68$ ), VOCs/ $\text{NO}_x$  ( $R = 0.51$ – $0.63$ ), and  $\text{NO}$  ( $R = 0.29$ – $0.54$ ). The model has negative mean biases by 22.6–36.8% for VOCs concentrations and positive biases by 26.6–67.1% for  $\text{NO}_x$  and  $\text{NO}_2$ . The modeled ratios of anthropogenic to total (anthropogenic + nature) VOCs range from 69.1% to 78.3%, lower than the observed ratios (81.2–92.6%) identified from the PMF analysis. Overall, the “Control” simulation reproduces the diversities in ozone and precursors at these five cities, despite the existence of systematic biases. Further comments on the model capability of  $\text{O}_3$ ,  $\text{NO}_x$  and different VOCs species are shown in Sect. 4.

To investigate the importance of local anthropogenic sources on city-level ozone, we conduct five sensitivity simulations of GEOS-Chem (xWH, xHS, xEZ, xXG and xHG, respectively), each by removing anthropogenic emissions in one of the five cities throughout the study period. This set of simulations is referred to as the “xLocal” case. The difference between “Control” and “xLocal” represents the contribution of a city’s local anthropogenic emissions to its ozone concentration. Ozone photochemistry is nonlinearly dependent on its precursors, adding uncertainties to the source attribution calculated by emission perturbation methods. Thus we use a linear weighting method to adjust all ozone attribution results (Ni et al., 2018). An example to determine the contribution from local anthropogenic emissions in WH is provided below (here Ci represents the sensitivity simulation for one of the five cities). The adjustment is performed for each grid cell. Equation (1) calculates the local contribution ( $\alpha$ ) to the sum of ozone from individual anthropogenic source regions and from natural sources. Equation (2) applies the fractional contribution  $\alpha$  to the total ozone in control simulation to obtain the final adjusted local contribution.

$$\alpha = \frac{\text{Con}(\text{Control}) - \text{Con}(\text{xWH})}{\sum_{i=1}^5 [\text{Con}(\text{Control}) - \text{Con}(\text{Ci})] + \text{Con}(\text{xWCC})} \quad (1)$$

$$C_{\text{WH}} = \alpha \times \text{Con}(\text{Control}) \quad (2)$$

Fig. 6a shows that local anthropogenic sources contribute 27.5%, 26.8%, 28.1%, 29.5% and 27.6% of MDA8 ozone averaged in May–June at WH, XG, HS, HG, and EZ, respectively. Furthermore, the cross-city ozone diversities (i.e., ozone at a city minus the 5-city mean) due to local anthropogenic emissions are 56.2–62.7% of the diversities in the “Control” simulation (Fig. 6b). These large local contributions suggest the necessity of accounting for local emission diversities in city-level ozone control.

We conduct two additional sensitivity simulations to further quantify the contributions of non-local anthropogenic emissions to city-level ozone. A “xWCC” simulation excludes anthropogenic emissions over the five cities in WCC together; thus the difference between “xLocal” and “xWCC” represents the effect of cross-city transboundary transport from other four cities of WCC on ozone at a given city. Table 2 shows that cross-city transboundary transport from other four cities of WCC (xLocal – xWCC) contribute 2.5%, 2.7%, 2.8%, 3.1% and 2.8% of ozone on MDA8 ozone at WH, XG, HS, HG, and EZ, respectively. This suggests a relatively weak effect of anthropogenic emissions from nearby cities, much weaker than local anthropogenic contributions (26.8%–29.5%).

A “Background” simulation removes all anthropogenic emissions within the nested domain (70°E–140°E, 15°N–55°N), representing the contribution of anthropogenic emissions outside Asia together with the contribution from global natural sources. The total “Background” contribution is simulated to be 48.9–51.6% (Table 2), as the most

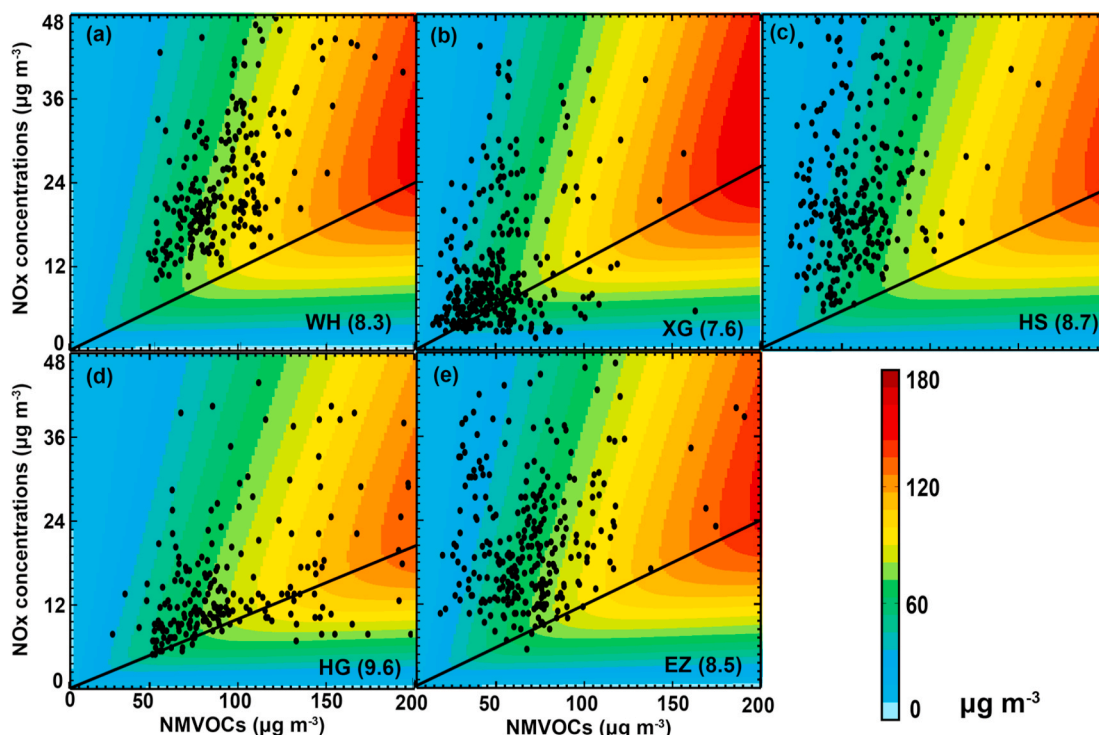


Fig. 3. The ozone-isopleth diagrams derived from DSMACC for the five cities. Also shown are the VOCs/NO<sub>x</sub> ratios (in parentheses) for the ridge lines (black lines). The black dots represent the hourly observed VOCs and NO<sub>x</sub> concentrations during the strong ozone photochemical buildup hours (10:00–15:00).

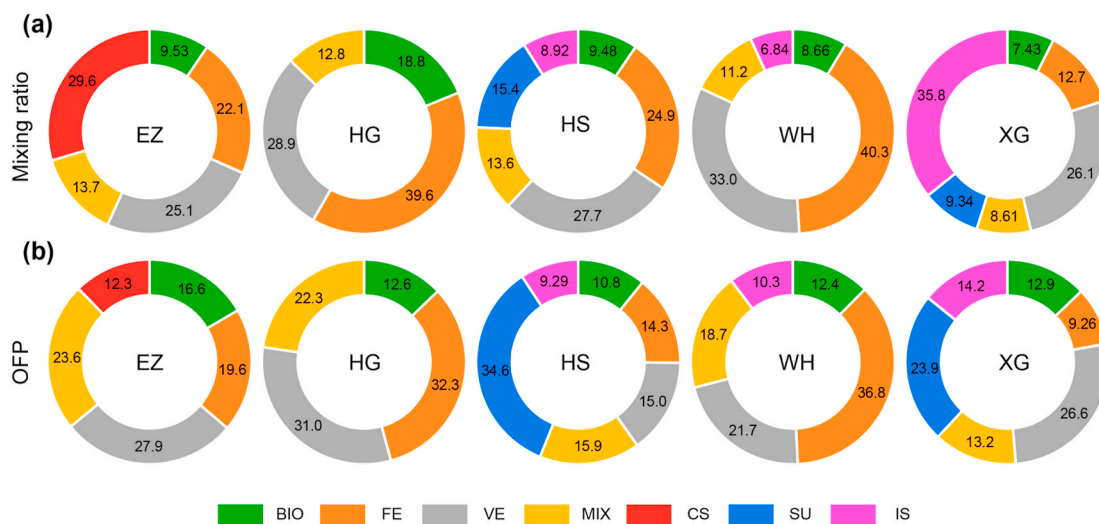


Fig. 4. Percentage contributions (%) of different VOC sources to the VOCs mixing ratio (a) and ozone formation potential (OFP, b) at each city. Sources include biogenic (BIO), fuel evaporation (FE), vehicle emissions (VE), mixed (MIX), combustion source (CS), solvent usage (SU), and industrial sources (IS).

dominant contributor to city-level ozone at any of the five cities. The difference between “xWCC” and “Background” represents the contribution of transboundary transport from non-WCC Asian regions, which ranges from 18.5 to 19.2% for the five cities. These results highlight the dominant roles of long-range transport and natural sources to city-level ozone, providing a theoretical limit for the achievable successfulness of local pollution control.

For the ozone episode on June 16 with the highest MDA8 ozone concentrations (37.9–71.9% higher than China’s Secondary Standard), the “Background” contributions to each city (46.4–48.2%) are lower than the average values (48.9–51.6%) over May–June (Fig. 6a). The modeled contributions of local anthropogenic emissions reach

30.8–32.0%, higher than mean contributions (26.8–29.5%) during May–June. The contributions of cross-city transboundary transport and non-WCC Asian regions are similar to their average contributions for May–June. These results show that the local anthropogenic contributions are more important during the ozone episodes, although local control would not fully remove the ozone exceedances in a city.

#### 4. Discussion

Our results show that in the urban agglomeration regions, although ozone pollution is of regional feature to a large extent, there are distinct city-level characteristics in ozone, NO<sub>x</sub>, VOCs/NO<sub>x</sub> ratio, and sources

**Table 2**

GEOS-Chem simulated percentage contributions of background ozone (including global natural sources and non-Asian anthropogenic emissions; defined as: Background/Control), non-WCC Asian anthropogenic emissions (defined as: (xWCC-Background)/Control), cross-city transport within WCC (defined as: (xLocal-xWCC)/Control), and local anthropogenic emissions (defined as: (Control-xLocal)/Control) to ozone at each city. All values are scaled to adjust for the effect of the nonlinear ozone chemistry on source attribution, such that the sum of all values in each row is equal to 100%.

Sites	Background	Non-WCC Asian	Cross-city transport within WCC	Local anthropogenic
WH	50.6%	19.1%	2.8%	27.5%
XG	51.6%	18.9%	2.7%	26.8%
HS	49.9%	19.2%	2.8%	28.1%
HG	48.9%	18.5%	3.1%	29.5%
EZ	50.5%	19.1%	2.8%	27.6%

**Table 3**

Anthropogenic emissions of ozone precursors (CO, NO<sub>x</sub> and VOCs) for the five cities in GEOS-Chem control simulation during May–June in 2018, averaged over the grids covered by the entire urban area of individual city.

Sites	CO (g m <sup>-2</sup> )	NO <sub>x</sub> (g m <sup>-2</sup> )	VOCs (g C m <sup>-2</sup> )
WH	219.09	19.72	7.17
XG	48.51	1.44	1.26
HS	60.70	1.93	1.61
HG	74.82	1.91	2.08
EZ	65.42	2.08	1.83

and ozone formation potential of VOCs. Removal of local anthropogenic emissions in a city alone would lower its ozone concentration by up to one third in the simulation, especially during ozone episodes. This provides an opportunity to effectively mitigate ozone pollution by local emission control actions, independent on regional and global collaborative actions that are often more difficult to be agreed upon and/or be implemented in practice.

In addition, although the ozone formation regime is VOC-limited on average for all cities studied here, there are substantial variabilities across the cities and days. This indicates that uniform local emission control actions by targeting VOCs alone may not be the most effective way to mitigate ozone at certain cities on certain days. Instead, continuous forecasts facilitated by measurements may be necessary to reduce ozone on a city-level and daily basis.

The relatively small ozone contribution (within 4%) from cross-city transport within WCC also implies that emission control collaborations within the urban agglomeration region alone may only have marginal usefulness in ozone mitigation. The regionally collaborative ozone control would be accomplished by reducing emissions of a much larger domain (e.g., the whole country of China) or even by reducing emissions worldwide, given the substantial long-range transboundary influences. China has implemented collaborative actions within each of a few key regions (e.g., Beijing-Tianjin-Hebei and the Yangtze River Delta) to mitigate particulate matter pollution. Expanding the collaboration

domains would be helpful to mitigate ozone pollution.

It should be noted the MIR method and PMF model both lead to the uncertainty of the OFP of each VOC source. For the MIR method, it takes into consideration the impacts of chemical mechanisms and VOCs/NO<sub>x</sub> ratios on ozone production, which may introduce some mechanism and simulation uncertainties. In addition, the MIR determined in one location may be different from that in another. For the uncertainty of PMF model, it comes from four assumptions: (1) source profiles do not change significantly over time; (2) species do not react chemically or undergo physical processes; (3) collected data are consistent with the conceptual model and represent the studied geographical area and (4) equivalent/comparable analytical methods are applied to the receptor site throughout the study (Belis et al., 2013). The photochemistry of VOCs in the ambient air make it difficult to separate and interpret the sources derived from PMF model (Yuan et al., 2012).

The GEOS-Chem model used in this study (the “Control” simulation) generally underestimates the observed ozone and VOCs concentrations, but has positive biases for NO<sub>x</sub> and NO<sub>2</sub> concentrations. The underestimate in VOCs and overestimate in NO<sub>x</sub> could be because anthropogenic emissions for ozone precursors used in the “Control” simulation are for the year of 2016. From 2016 to 2018, the simulated year here, anthropogenic NO<sub>x</sub> emissions in Central China have declined substantially, due to implementation of stringent NO<sub>x</sub> emission control measures (China State Council, 2011, 2016) for the 13th Five-Year Plan. Meanwhile, anthropogenic emissions of VOCs have increased continuously (Li et al., 2017; Zheng et al., 2018), resulting in higher ozone production than simulated in the “Control” case. Also, the VOCs underestimation could be explained by the relative coarse grid resolution of 0.25° for localized anthropogenic emissions, which would be caused to the artificial dispersion and smoothed VOCs concentrations at each site with respect to chemical ozone formation. It is also reported by Yan et al. (2016). In addition, the decline in particulate matter pollution from 2016 to 2018 may have also led to stronger radiation and higher radical concentrations for near-surface ozone formation (Li et al., 2019c), which is not accounted for here. The NO<sub>x</sub> and VOCs biases from anthropogenic emissions may affect our simulations and ozone attribution results to some extent.

The differences between observed and modeled VOC species are another limitation of our simulations and ozone attribution analysis here. Specifically, the measured species (listed in the captions of Figs. S2–S6) do not fully match the modeled species (including benzene, toluene, xylene, isoprene, other alkenes, ethane, propane, other alkanes, formaldehyde, other aldehydes, acetone and methyl ethyl ketone). The speciation assumption partly accounts for the biases in the modeled VOCs concentrations and anthropogenic to total VOC ratios shown in Sect. 3.3.

#### Credit author contribution statement

**Yingying Yan:** Data curation, Formal analysis, Writing - original draft, conceived and designed the research, performed the data processing, model simulations, and analyses, wrote the paper with input

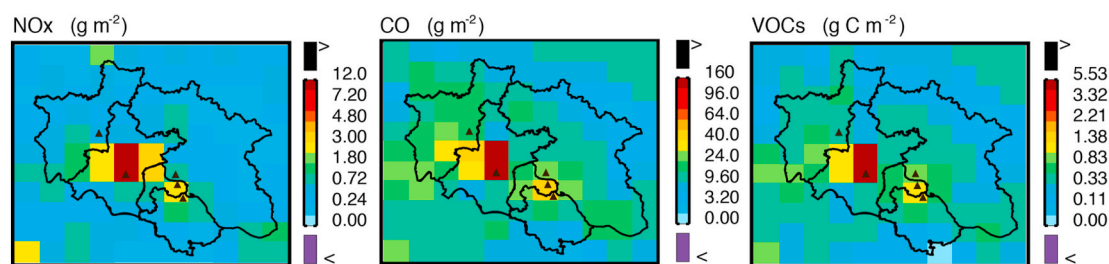


**Fig. 5.** The actual boundaries of these five cities with the GEOS-Chem model grid cells and MEIC emission shown explicitly, also shown are the measurement sites at five cities.

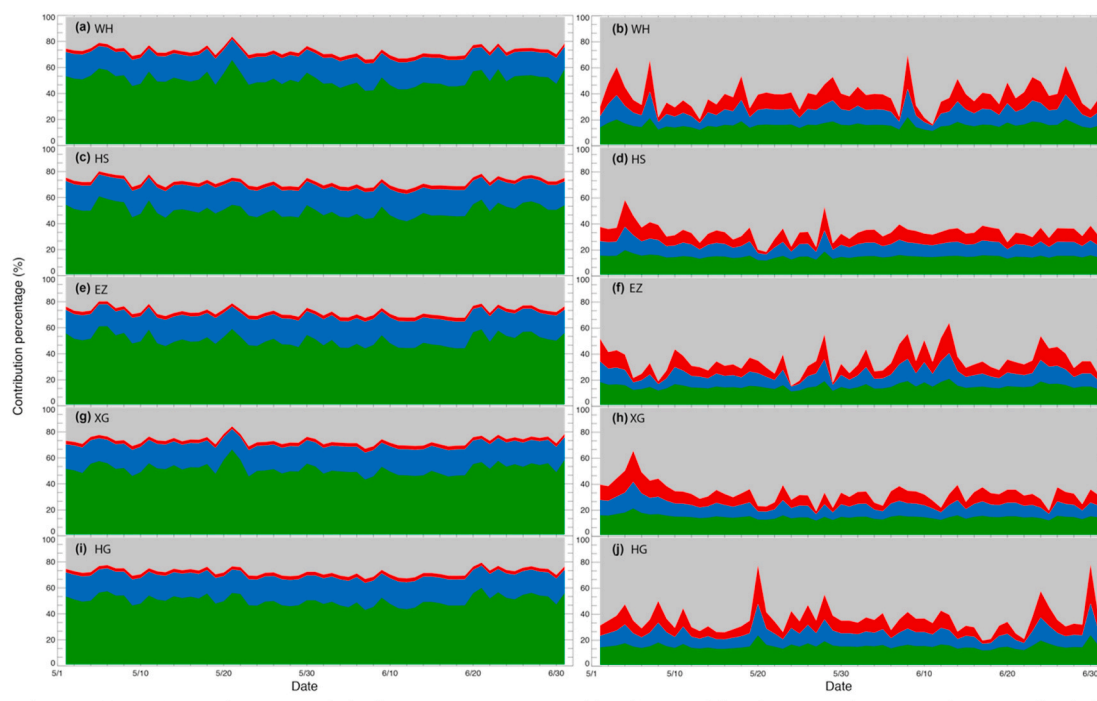


**Fig. 6.** GEOS-Chem modeled percentage contributions of background ozone (green shade), non-WCC Asian anthropogenic sources (blue shade), cross-city transport within WCC (red shade), and local anthropogenic emissions (grey shade) to (a, c, e, g and i) ozone and (b, d, f, h and j) cross-city ozone diversity for each city. (For interpretation of the references to colour in this figure legend, the reader is referred to the Web version of this article.)

from all authors. **Huang Zheng:** assisted in the PMF model simulations. **Shaofei Kong:** Data curation, Formal analysis, Writing - original draft, Funding acquisition, conceived and designed the research, performed the data processing, model simulations, and analyses, wrote the paper with input from all authors, contributed the funding acquisition. **Jintai Lin:** Data curation, Formal analysis, Writing - original draft, conceived and designed the research, performed the data processing, model simulations, and analyses, wrote the paper with input from all authors. **Nan Chen:** Data curation, provided the observation data over WCC. **Tianliang Zhao:** Funding acquisition, contributed the funding acquisition. **Shihua Qi:** Funding acquisition, contributed the funding acquisition.

#### Declaration of competing interest

We wish to confirm that there are no known conflicts of interest associated with this publication.

#### Acknowledgement

This study was financially supported by the Key Program of Ministry of Science and Technology of the People's Republic of China (2016YFA0602002; 2017YFC0212602), the Key Program for Technical Innovation of Hubei Province (2017ACA089), the National Natural Science Foundation of China (41830965; 41775115; 41905112). The research was also funded by the Fundamental Research Funds for the Central Universities, China University of Geosciences (Wuhan) (G1323519230; 201616; 201802; CUG190609) and the Start-up Foundation for Advanced Talents (162301182756).

#### Appendix A. Supplementary data

Supplementary data to this article can be found online at <https://doi.org/10.1016/j.atmosenv.2020.118005>.

#### Author declaration

We wish to confirm that there are no known conflicts of interest associated with this publication.

We confirm that the manuscript has been read and approved by all named authors and that there are no other persons who satisfied the criteria for authorship but are not listed. We further confirm that the order of authors listed in the manuscript has been approved by all of us.

We confirm that we have given due consideration to the protection of intellectual property associated with this work and that there are no impediments to publication, including the timing of publication, with respect to intellectual property. In so doing we confirm that we have followed the regulations of our institutions concerning intellectual property.

We understand that the Corresponding Author is the sole contact for the Editorial process (including Editorial Manager and direct communications with the office). He/she is responsible for communicating with the other authors about progress, submissions of revisions and final approval of proofs. We confirm that we have provided a current, correct email address which is accessible by the Corresponding Author and which has been configured to accept email from [yanyy09@163.com](mailto:yanyy09@163.com).

#### References

- Belis, C.A., Karagulian, F., Larsen, B.R., Hopke, P.K., 2013. Critical review and meta-analysis of ambient particulate matter source apportionment using receptor models in Europe. *Atmos. Environ.* 69, 94–108. <https://doi.org/10.1016/j.atmosenv.2012.11.009>.
- Bon, D.M., Ulbrich, I.M., de Gouw, J.A., Warneke, C., Kuster, W.C., Alexander, M.L., Baker, A., Beyersdorf, A.J., Blake, D., Fall, R., Jimenez, J.L., Herndon, S.C., Huey, L. G., Knighton, W.B., Ortega, J., Springston, S., Vargas, O., 2011. Measurements of volatile organic compounds at a suburban ground site (T1) in Mexico City during the MILAGRO 2006 campaign: measurement comparison, emission ratios, and source attribution. *Atmos. Chem. Phys.* 11 (6), 2399–2421. <https://doi.org/10.5194/acp-11-2399-2011>.
- Cheung, V.T.F., Wang, T., 2001. Observational study of ozone pollution at a rural site in the Yangtze Delta of China. *Atmos. Environ.* 35, 4947–4958.
- China State Council, 2011. 12<sup>th</sup> Five-Year Plan on National Economy and Social Development of the People's Republic of China available at: [http://www.gov.cn/2011lh/content\\_1825838.htm](http://www.gov.cn/2011lh/content_1825838.htm) (in Chinese).

- China State Council, 2016. 13<sup>th</sup> Five-Year Plan on National Economy and Social Development of the People's Republic of China available at: [http://www.gov.cn/zhe/ncge/content/2017-01/05/content\\_5156789.htm](http://www.gov.cn/zhe/ncge/content/2017-01/05/content_5156789.htm) (in Chinese).
- Colette, A., Granier, C., Hodnebrog, O., Jakobs, H., Maurizi, A., Nyiri, A., Bessagnet, B., D'Angiola, A., D'Isidoro, M., Gauss, M., Meleux, F., Memmesheimer, M., Mieville, A., Rouil, L., Russo, F., Solberg, S., Stordal, F., Tampieri, F., 2011. Air quality trends in Europe over the past decade: a first multi-model assessment. *Atmos. Chem. Phys.* 11, 11657–11678. <https://doi.org/10.5194/acp-11-11657-2011>.
- Derstroff, B., Hüser, I., Sander, R., Bourtsoukidis, E., Crowley, J.N., Fischer, H., Gromov, S., Harder, H., Kesselmeier, J., Lelieveld, J., Mallik, C., Martinez, M., Novelli, A., Parchatka, U., Phillips, G.J., Sauvage, C., Schuladen, J., Stöner, C., Tomsche, L., Williams, J., 2016. Volatile organic compounds (VOCs) in photochemically aged air from the Eastern and Western Mediterranean. *Atmos. Chem. Phys. Discuss.* 1–44. <https://doi.org/10.5194/acp-2016-746>.
- Derwent, R.G., Witham, C.S., Utembe, S.R., Jenkin, M.E., Passant, N.R., 2010. Ozone in Central England: the impact of 20 years of precursor emission controls in Europe. *Environ. Sci. Pol.* 13, 195–204. <https://doi.org/10.1016/j.envsci.2010.02.001>.
- EEA, 2007. *Air Pollution in Europe 1990–2004*. European Environment Agency, Copenhagen.
- EEA, 2009. *Assessment of Ground-Level Ozone in EEA Member Countries, with a Focus on Long-Term Trends*.
- EEA, 2011. *Air quality in Europe — 2011 report*. EEA 80.
- EEA, 2017. *Air Quality in Europe-2017 Report*. Publications Office of the European Union, Luxembourg, ISBN 978-92-9213-920-9, p. 74. EEA Report, No 13/2017. (Accessed 15 March 2018). available at: <https://www.eea.europa.eu/publications/air-quality-in-europe-2017>.
- Fowler, D., Brunkreef, B., Fuzzi, S., Monks, P.S., Sutton, M.A., Brasseur, G.P., Friedrich, R., Passante, L.G., Jimenez-Mingo, J.M., 2013. *Research Findings in Support of the EU Air Quality Review*. Publications office of the European Union, Luxembourg.
- Geng, Fuhai, Zhao, Chunsheng, Tang, Xu, et al., 2007. Analysis of ozone and VOCs measured in Shanghai: a case study. *Atmos. Environ.* 41, 989–1001.
- Geng, F.H., Cai, C.J., Tie, X., et al., 2010. Analysis of VOC emissions using PCA/APCS receptor model at city of Shanghai, China. *J. Atmos. Chem.* 62, 229–247.
- Gentner, D.R., Harley, R.A., Miller, A.M., Goldstein, A.H., 2009. Diurnal and seasonal variability of gasoline-related volatile organic compound emissions in Riverside, California. *Environ. Sci. Technol.* 43 (12), 4247–4252. <https://doi.org/10.1021/es9006228>.
- Gressent, A., Sauvage, B., Cariolle, D., Evans, M., Leriche, M., Mari, C., Thouret, V., 2016. Modeling lightning-NOx chemistry on a sub-grid scale in a global chemical transport model. *Atmos. Chem. Phys.* 16, 5867–5889. <https://doi.org/10.5194/acp-16-5867-2016>.
- Guo, H., Wang, T., Louie, P.K.K., 2004. Source apportionment of ambient non-methane hydrocarbons in Hong Kong: application of a principal component analysis/absolute principal component scores (PCA/APCS) receptor model. *Environ. Pollut.* 129, 489–498.
- Guo, H., Wang, T., Blake, D.R., Simpson, I.J., Kwok, Y.H., Li, Y.S., 2006. Regional and local contributions to ambient non-methane volatile organic compounds at a polluted rural/coastal site in Pearl River Delta, China. *Atmos. Environ.* 40, 2345–2359.
- Han, S., Bian, H., Feng, Y., Liu, A., Li, X., Zeng, F., Zhang, X., 2011. Analysis of the Relationship between O<sub>3</sub>, NO and NO<sub>2</sub> in Tianjin, China. *Aerosol Air Qual. Res.* 11, 128–139. <https://doi.org/10.4209/aaqr.2010.07.0055>.
- HTAP, 2010. *Hemispheric Transport of Air Pollution*. UNECE, Geneva.
- Jobson, B.T., 2004. Hydrocarbon source signatures in Houston, Texas: influence of the petrochemical industry. *J. Geophys. Res.* 109 (D24) <https://doi.org/10.1029/2004JD004887>.
- Kaltsonoudis, C., Kostenidou, E., Florou, K., Psychoudaki, M., Pandis, S.N., 2016. Temporal variability and sources of VOCs in urban areas of Eastern Mediterranean. *Atmos. Chem. Phys.* 1–33. <https://doi.org/10.5194/acp-2016-358>.
- Lelieveld, J., Evans, J.S., Fnais, M., Giannadaki, D., Pozzer, A., 2015. The contribution of outdoor air pollution sources to premature mortality on a global scale. *Nature* 525, 367–371.
- Li, M., Liu, H., Geng, G., Hong, C., Liu, F., Song, Y., Tong, D., Zheng, B., Cui, H., Man, H., Zhang, Q., He, K., 2017. Anthropogenic emission inventories in China: a review. *Natl. Sci. Rev.* 4 (6), 834–866. <https://doi.org/10.1093/nsr/nwx150>.
- Li, B., Ho, S.S.H., Gong, S., Ni, J., Li, H., Han, L., Yang, Y., Qi, Y., Zhao, D., 2019a. Characterization of VOCs and their related atmospheric processes in a central Chinese city during severe ozone pollution periods. *Atmos. Chem. Phys.* 19, 617–638. <https://doi.org/10.5194/acp-19-617-2019>.
- Li, B., Ho, S.S.H., Gong, S., Ni, J., Li, H., Han, L., Yang, Y., Qi, Y., Zhao, D., 2019b. Characterization of VOCs and their related atmospheric processes in a central Chinese city during severe ozone pollution periods. *Atmos. Chem. Phys.* 19, 617–638. <https://doi.org/10.5194/acp-19-617-2019>.
- Li, K., Jacob, D.J., Liao, H., Shen, L., Zhang, Q., Bates, K.H., 2019c. Anthropogenic drivers of 2013–2017 trends in summer surface ozone in China. *Proc. Natl. Acad. Sci. U.S.A.* 116 (2), 422–427. <https://doi.org/10.1073/pnas.1812168116>.
- Lin, J.-T., McElroy, M.B., 2010. Impacts of boundary layer mixing on pollutant vertical profiles in the lower troposphere: implications to satellite remote sensing. *Atmos. Environ.* 44, 1726–1739. <https://doi.org/10.1016/j.atmosenv.2010.02.009>.
- Lin, J.-T., Wuebbles, D.J., Liang, X.Z., 2008. Effects of intercontinental transport on surface ozone over the United States: present and future assessment with a global model. *Geophys. Res. Lett.* 35, L02805. <https://doi.org/10.1029/2007gl031415>.
- Liu, Y., Shao, M., Fu, L., Lu, S., Zeng, L., Tang, D., 2008. Source profiles of volatile organic compounds (VOCs) measured in China: Part I. *Atmos. Environ.* 42 (25), 6247–6260. <https://doi.org/10.1016/j.atmosenv.2008.01.070>.
- Lyu, X.P., Chen, N., Guo, H., Zhang, W.H., Wang, N., Wang, Y., Liu, M., 2016. Ambient volatile organic compounds and their effect on ozone production in Wuhan, central China. *Sci. Total Environ.* 541, 200–209. <https://doi.org/10.1016/j.scitotenv.2015.09.093>.
- Mao, J.Q., Paulot, F., Jacob, D.J., Cohen, R.C., Crounse, J.D., Wennberg, P.O., Keller, C.A., Hudman, R.C., Barkley, M.P., Horowitz, L.W., 2013. Ozone and organic nitrates over the eastern United States: sensitivity to isoprene chemistry. *J. Geophys. Res.* Atmos. 118, 11256–11268. <https://doi.org/10.1002/jgrd.50817>.
- McCarthy, M.C., Akilu, Y.A., Brown, S.G., Lyder, D.A., 2013. Source apportionment of volatile organic compounds measured in Edmonton, Alberta. *Atmos. Environ. Times* 81, 504–516. <https://doi.org/10.1016/j.atmosenv.2013.09.016>.
- McLinden, C.A., Olsen, S.C., Hannegan, B., Wild, O., Prather, M.J., Sundet, J., 2000. Stratospheric ozone in 3-D models: a simple chemistry and the cross-tropopause flux. *J. Geophys. Res. Atmos.* 105, 14653–14665. <https://doi.org/10.1029/2000jd900124>.
- Monks, P.S., Archibald, A.T., Colette, A., Cooper, O., Coyle, M., Derwent, R., Fowler, D., Granier, C., Law, K.S., Mills, G.E., Stevenson, D.S., Tarasova, O., Thouret, V., von Schneidmesser, E., Sommariva, R., Wild, O., Williams, M.L., 2015. Tropospheric ozone and its precursors from the urban to the global scale from air quality to short-lived climate forcer. *Atmos. Chem. Phys.* 15, 8889–8973. <https://doi.org/10.5194/acp-15-8889-2015>.
- Ni, R.J., Lin, J.T., Yan, Y.Y., Lin, W., 2018. Foreign and domestic contributions to springtime ozone over China. *Atmos. Chem. Phys.* 18, 11447–11469. <https://doi.org/10.5194/acp-18-11447-2018>.
- Ou, J.M., Yuan, Z.B., Zheng, J.Y., Huang, Z.J., Shao, M., Li, Z.K., Huang, X.B., Guo, H., Louie, P.K.K., 2016. Ambient ozone control in a photochemically active region: short-Term despike or long-Term attainment? *Environ. Sci. Technol.* 50, 5720–5728. <https://doi.org/10.1021/acs.est.6b00345>.
- Royal Society, 2008. *Ground-level Ozone in the 21st Century: Future Trends, Impacts and Policy Implications*. The Royal Society, London.
- So, K.L., Wang, T., 2003. On the local and regional influence on ground-level ozone concentrations in Hong Kong. *Environ. Pollut.* 123, 307–317.
- So, K.L., Wang, T., 2004. C3–C12 non-methane hydrocarbons in subtropical Hong Kong: spatial-temporal variations, source-receptor relationships and photochemical reactivity. *Sci. Total Environ.* 328, 161–174.
- Song, M., Tan, Q., Feng, M., Qu, Y., Liu, X., An, J., Zhang, Y., 2018. Source apportionment and secondary transformation of atmospheric nonmethane hydrocarbons in Chengdu, Southwest China. *J. Geophys. Res. Atmospheres*. <https://doi.org/10.1029/2018JD028479>.
- Sun, L., Xue, L., Wang, Y., Li, L., Lin, J.-T., Ni, R.J., Yan, Y.Y., Chen, L.L., Li, J., Zhang, Q., Wang, W., 2019. Impacts of meteorology and emissions on summertime surface ozone increases over central eastern China between 2003 and 2015. *Atmos. Chem. Phys.* 19, 1455–1469. <https://doi.org/10.5194/acp-19-1455-2019>.
- Tai, A.P.K., val Martin, M., Heald, C.L., 2004. Threat to future global food security from climate change and ozone air pollution. *Nat. Clim. Change*. <https://doi.org/10.1038/nclimate2317>.
- Verstraeten, W.W., Neu, J.L., Williams, J.E., Bowman, K.W., Worden, J.R., Boersma, K.F., 2015. Rapid increases in tropospheric ozone production and export from China. *Nat. Geosci.* 8 (9), 690.
- Wang, H., 2014. Source profiles and chemical reactivity of volatile organic compounds from solvent use in Shanghai, China. *Aerosol Air Qual. Res.* 14 (1), 301–310. <https://doi.org/10.4209/aaqr.2013.03.0064>.
- Wang, T., Nie, W., Gao, J., Xue, L.K., Gao, X.M., Wang, X.F., et al., 2010. Air quality during the 2008 Beijing Olympics: secondary pollutants and regional impact. *Atmos. Chem. Phys.* 10, 7603–7615.
- Wilson, R.C., Fleming, Z.L., Monks, P.S., Clain, G., Henne, S., Konovalov, I.B., Szopa, S., Menut, L., 2012. Have primary emission reduction measures reduced ozone across Europe? An analysis of European rural background ozone trends 1996–2005. *Atmos. Chem. Phys.* 12, 437–454. <https://doi.org/10.5194/acp-12-437-2012>.
- Xue, L., Wang, T., Louie, P.K.K., Luk, C.W.Y., Blake, D.R., Xu, Z., 2014. Increasing external effects negate local efforts to control ozone air pollution: a case study of Hong Kong and implications for other Chinese cities. *Environ. Sci. Technol.* 48, 10769–10775.
- Yan, Y.Y., Lin, J.T., He, C.L., 2018a. Ozone trends over the United States at different times of day. *Atmos. Chem. Phys.* 18, 1185–1202. <https://doi.org/10.5194/acp-18-1185-2018>.
- Yan, Y.Y., Pozzer, A., Ojha, N., Lin, J.T., Lelieveld, J., 2018b. Analysis of European ozone trends in the period 1995–2014. *Atmos. Chem. Phys.* 18, 5589–5605. <https://doi.org/10.5194/acp-18-5589-2018>.
- Yan, Y.-Y., Lin, J.-T., Pozzer, A., Kong, S., Lelieveld, J., 2019a. Trend reversal from high-to-low and from rural-to-urban ozone concentrations over Europe. *Atmos. Environ.* 213, 25–36. <https://doi.org/10.1016/j.atmosenv.2019.05.067>.
- Yan, Y., Cabrera-Perez, D., Lin, J., Pozzer, A., Hu, L., Millet, D.B., Porter, W.C., Lelieveld, J., 2019b. Global tropospheric effects of aromatic chemistry with the SAPRC-11 mechanism implemented in GEOS-Chem version 9-02. *Geosci. Model Dev.* (GMD) 12, 111–130. <https://doi.org/10.5194/gmd-12-111-2019>.
- Yan, Y.Y., Lin, J.T., Pozzer, A., Kong, S.F., Lelieveld, J., 2019c. Trend reversal from high-to-low and from rural-to-urban ozone concentrations over Europe. *Atmos. Environ.* 213, 25–36. <https://doi.org/10.1016/j.atmosenv.2019.05.067>.
- Yu, C., Zhao, T., Bai, Y., Zhang, L., Kong, S., Yu, X., He, J., Cui, C., Yang, J., You, Y., Ma, G., Wu, M., Chang, J., 2020. Heavy air pollution with a unique "non-stagnant" atmospheric boundary layer in the Yangtze River middle basin aggravated by regional transport of PM<sub>2.5</sub> over China. *Atmos. Chem. Phys.* 20, 7217–7230. <https://doi.org/10.5194/acp-20-7217-2020>.

- Yuan, B., Shao, M., Lu, S., Wang, B., 2010. Source profiles of volatile organic compounds associated with solvent use in Beijing, China. *Atmos. Environ. Times* 44 (15), 1919–1926. <https://doi.org/10.1016/j.atmosenv.2010.02.014>.
- Yuan, B., Shao, M., de Gouw, J., Parrish, D.D., Lu, S., Wang, M., Zeng, L., Zhang, Q., Song, Y., Zhang, J., Hu, M., 2012. Volatile organic compounds (VOCs) in urban air: how chemistry affects the interpretation of positive matrix factorization (PMF) analysis. *J. Geophys. Res. Atmos.* 117 <https://doi.org/10.1029/2012JD018236>.
- Zhang, Y., Wang, X., Zhang, Z., Lü, S., Shao, M., Lee, F.S.C., Yu, J., 2013. Species profiles and normalized reactivity of volatile organic compounds from gasoline evaporation in China. *Atmos. Environ.* 79, 110–118. <https://doi.org/10.1016/j.atmosenv.2013.06.029>.
- Zhang, J., Tian, W., Xie, F., Li, Y., Wang, F., Huang, J., Tian, H., 2015. Influence of the El Niño southern oscillation on the total ozone column and clear-sky ultraviolet radiation over China. *Atmos. Environ.* 120, 205–216.
- Zhang, Q., Wu, L., Fang, X., Liu, M., Zhang, J., Shao, M., Lu, S., Mao, H., 2018. Emission factors of volatile organic compounds (VOCs) based on the detailed vehicle classification in a tunnel study. *Sci. Total Environ.* 624, 878–886. <https://doi.org/10.1016/j.scitotenv.2017.12.171>.
- Zhang, Jiankai, Tian, Wenshou, et al., 2018. Stratospheric ozone loss over the Eurasian continent induced by the polar vortex shift. *Nat. Commun.* 9 (1), 206.
- Zheng, H., Kong, S., Xing, X., Mao, Y., Hu, T., Ding, Y., Li, G., Liu, D., Li, S., Qi, S., 2018a. Monitoring of volatile organic compounds (VOCs) from an oil and gas station in northwest China for 1 year. *Atmos. Chem. Phys.* 18 (7), 4567–4595. <https://doi.org/10.5194/acp-18-4567-2018>.
- Zheng, H., Kong, S., Wu, F., Cheng, Y., Niu, Z., Zheng, S., Yang, G., Yao, L., Yan, Q., Wu, J., Zheng, M., Chen, N., Xu, K., Yan, Y., Liu, D., Zhao, D., Zhao, T., Bai, Y., Li, S., Qi, S., 2019. Intra-regional transport of black carbon between the south edge of the North China Plain and central China during winter haze episodes. *Atmos. Chem. Phys.* 19, 4499–4516. <https://doi.org/10.5194/acp-19-4499-2019>.
- Zheng, B., Tong, D., Li, M., Liu, F., Hong, C., Geng, G., Li, H., Li, X., Peng, L., Qi, J., Yan, L., Zhang, Y., Zhao, H., Zheng, Y., He, K., Zhang, Q., 2018. Trends in China's anthropogenic emissions since 2010 as the consequence of clean air actions. *Atmos. Chem. Phys. Discuss.* 18, 14095–14111. <https://doi.org/10.5194/acp-18-14095-2018>.